PROCEEDINGS OF SCIENCE

ONLINE ICRC 2021
THE ASTROPARTICLE PHYSICS CONFERENCE
Berlin | Germany
37th International Cosmic Ray Conference
12–23 July 2021

Test-Particle Simulations of SEPs Originating from an Expanding Shock-like Source

A Hutchinson,[a,*] **S. Dalla,**[a] **T. Laitinen**[a] **and C. O. G. Waterfall**[a]

[a] *Jeremiah Horrocks Institute, University of Central Lancashire, Preston, PR1 2HE, UK*

E-mail: AHutchinson3@uclan.ac.uk

Solar Energetic Particles (SEPs) are known to be accelerated at Coronal Mass Ejection (CME)-driven interplanetary shocks. Traditionally their propagation has been described via focussed transport approaches, limited to 1 or 2 spatial dimensions. We use 3D test particle simulations, which naturally incorporate the effect of drifts, to simulate the propagation of SEPs from a moving shock-like source. We investigate the effect of an expanding shock-like source propagating through interplanetary space, as opposed to an SEP source within the corona, on the observable properties of SEPs at 1 au and at locations nearer the Sun. We derive intensity profiles, anisotropies and longitudinal and latitudinal distribution of SEPs, with the aim of supporting observations from Solar Orbiter and Parker Solar Probe.

37th International Cosmic Ray Conference (ICRC 2021)
July 12th – 23rd, 2021
Online – Berlin, Germany

*Presenter

PoS(ICRC2021)1313

1. Introduction

Energetic protons are thought to be accelerated by CME-driven shocks near to the Sun and in interplanetary space, and by solar flares [7, 10]. There is a lack of knowledge of observable parameters that characterise specific distributions of particle injection from CME-driven shocks. With the launch of new spacecraft such as *Solar Orbiter* and *Parker Solar Probe* that observe these protons at radial distances close to the Sun ($\sim$ 0.3 au) we have a new perspective of in-situ energetic particle observations at our disposal to help identify the properties of a shock-injected particle population.

The particle injection from a CME-driven shock is temporally extended, especially for low energy particles [7] and the injection evolves with radial position of the shock with maximum injection located close to the Sun [7, 9]. The particle acceleration efficiency of CME-driven shocks is thought to be non-uniform across the shock front, with the nose of the shock being the most efficient and decreasing towards the flanks of the shock [9].

The test-particle code we use was developed by Marsh et al (2013) [6], where they used instantaneous near-Sun injections to study the propagation of Solar Energetic Particles (SEPs) and their associated drifts in interplanetary space. All other previous work with this test-particle code also considered instantaneous injections close to the Sun, e.g. Dalla et al (2020) [2] investigated the propagation of SEPs through interplanetary space in the presence of the heliospheric current sheet.

In this preliminary work we have developed a radially extended injection that is non-uniform in longitude and latitude that approximates particle injection from a CME-driven shock source. We consider the effects of the extended injection on intensity and anisotropy profiles of particles detected at 0.3 and 1.0 au. By considering the observable parameters close to the Sun (0.3 au) we aim to support observations from new spacecraft such as *Solar Orbiter* and *Parker Solar Probe*.

2. Injection Method

Previous work using this test-particle code have assumed an instantaneous injection at a fixed radial distance close to the Sun [1, 2, 6]. We use the same test-particle code but with a new method of particle injection which approximates an injection from a CME-driven shock. This differs from the previous instantaneous injection close to the Sun by extending the injection in time as the shock propagates outwards. We also consider variations in the longitudinal and latitudinal particle acceleration efficiency across the shock.

We consider a $50^\circ \times 50^\circ$ segment of a sphere to represent the particle-injecting shock, where we inject a mono-energetic population of one hundred thousand 100 MeV protons.

2.1 Radial and Temporal Injection

We assume that the CME-driven shock is formed at a heliocentric radial distance of 1.20 $R_\odot$, which corresponds to the median shock formation position determined by Gopalswamy et. al. (2013) [5], with an initial radial speed of 1500 km s^{-1}. This radial distance is the minimum injection position for the protons, however the injection function rises to a peak at a larger radial distance to account for the time required to accelerate the protons to 100 MeV before injection. We choose r_i = 100 $R_\odot$ to be the final position of particle injection and we assume that no particles

are accelerated beyond this distance. Note we do not model the acceleration process itself and the injected particles do not interact with the shock.

We derive an injection function by first specifying its variation with r, characterised by a fast rise to peak injection and a subsequent decay until the final injection position, according the the following injection function:

$$N(r_i) = \frac{A}{(r - r_{ini})^B} \exp\left(\frac{-C}{(r - r_{ini})}\right) \tag{1}$$

where A, B and C are positive constants, r_{ini} is the initial radial position of particle injection (1.2 $R_\odot$, i.e. the initial position of the shock), r is the radial distance from the Sun and $N(r)$ is the number of particles injected at the radial position r. For the values of the constants that we use the radial injection function peaks at 5.0 $R_\odot$. The radial injection described by Equation 1 can be seen in the left panel of Figure 1.

Starting from $N(r)$ we can determine the number of protons injected versus time by considering the motion of the shock. Therefore, by specifying the speed of the shock we can determine what the injection profile looks like with respect to time. The peak in injection at 5 $R_\odot$ occurs at $\sim$ 29.5 minutes, accounting for constant shock-deceleration as determined by Gopalswamy et al (2001) [4]. The profile of injection can be seen in Figure 1 (right panel).

2.2 Variation of Injection Efficiency Along the Shock Front

We incorporate longitudinal and latitudinal variations in the particle injection efficiency across the shock by considering Gaussian distributions in longitude and the sine of latitude. We use the sine of latitude to ensure that the protons are uniformly distributed on the spherical segment that represents the shock. We centre the shock at 0 degrees longitude and 15 degrees latitude so that the CME is located in the typical latitude range where CMEs originate [8]. The distributions in longitude and latitude are visible in Figure 2 for a standard deviation $\sigma = 10°$. Note that we consider

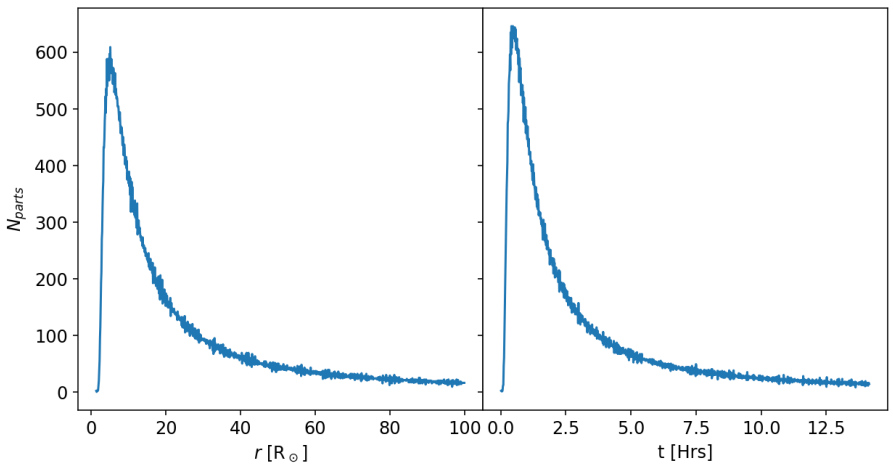

Figure 1: The radial and temporal distributions of particle injection for the simulations that considers a CME-driven shock with a radial speed of 1500 km s^{-1} at 1.2 $R_\odot$. The radial distribution follows Equation 1.

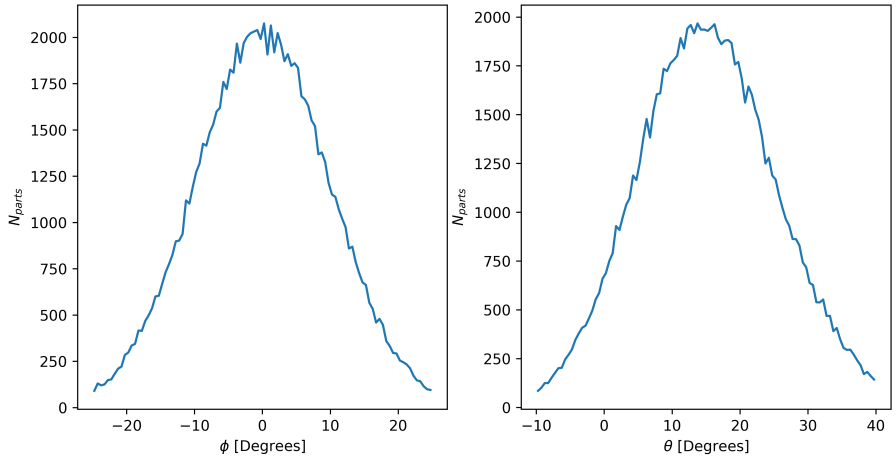

Figure 2: The longitudinal (left) and latitudinal (right) injection distributions, centred on the shock nose at (0°,15°). Both longitudinal and latitudinal distributions here have $\sigma = 10°$.

identical Gaussians (same σ) for both longitudinal and latitudinal variations in shock acceleration efficiency.

3. Results

3.1 Instantaneous vs Extended Injections

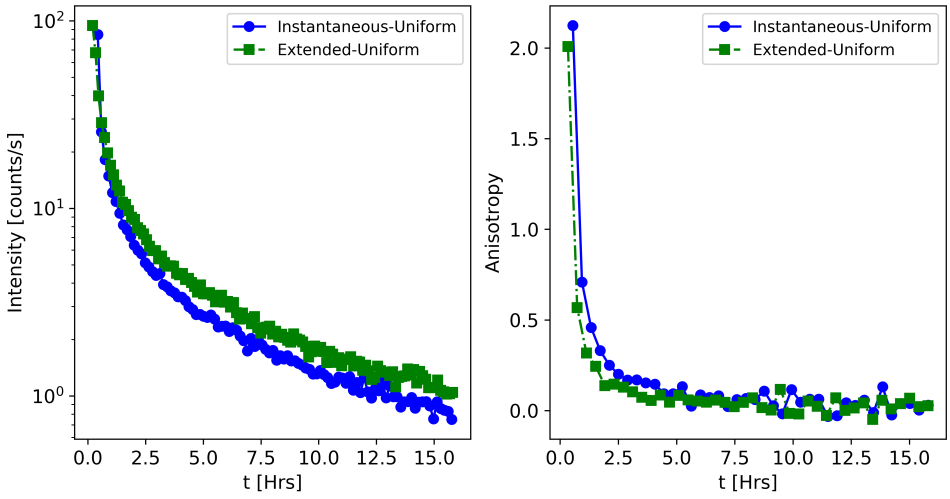

Figure 3: The intensity (left) and the anisotropy (right) profiles of 100 MeV protons at 1 au for a 50 x 50 degree observation tile centred at the initially magnetically well-connected region for the first 16 hours of simulations with an instantaneous injection at 2.0 $R_\odot$ (blue circles), and an injection extended in time corresponding to the $N(t)$ profile displayed in Figure 1 (green squares). Both injections spanned 50 degrees in longitude and latitude and the number of injected particles are the same and are uniform across the shock front. The simulations considered pitch angle scattering described a mean free path of $\lambda = 1.0$ au.

To compare the intensity and anisotropy profiles for the instantaneous and extended injections we consider a 50x50 degree collecting tile at 1 au, centred on the initially magnetically well-connected flux tubes. These can be seen in Figure 3. The instantaneous injection occurs at $r = 2.0$ $R_\odot$ at $t = 0$ and the extended occurs according to the description in Section 2. The extended injection results in slightly larger peak intensities and a more gradual decay in the intensity profile.

The instantaneous injection has a slightly larger anisotropy compared to the extended injection. The particles that are injected at greater distances from the solar surface during the extended injection have focussed less than those injected closer to the Sun in the instantaneous injection, but the effect on the anisotropy profile is minor.

3.2 Uniform vs Gaussian Efficiency Across the Shock

An important parameter to consider is the longitudinal and latitudinal variation of the injection efficiency along the shock front. We consider a) a shock with uniform injection, and Gaussian injections with b) $\sigma = 10°$, and c) $\sigma = 20°$ for a shock width of 50° in longitude and latitude. Note that we inject the same number of particles in all injections, but they are distributed differently across the shock front. We compare the intensity profiles at the initially magnetically well-connected region at 1 au in Figure 4 for the extended injections, considering a 25×25 degree collecting tile. The most shock-nose skewed injection ($\sigma = 10°$) results in consistently larger intensities compared to the more uniformly distributed injections. The most shock-nose skewed injection has a peak intensity that is ~ 4 times greater than the uniformly distributed injection and ~ 3 times larger than the $\sigma = 20°$ injection.

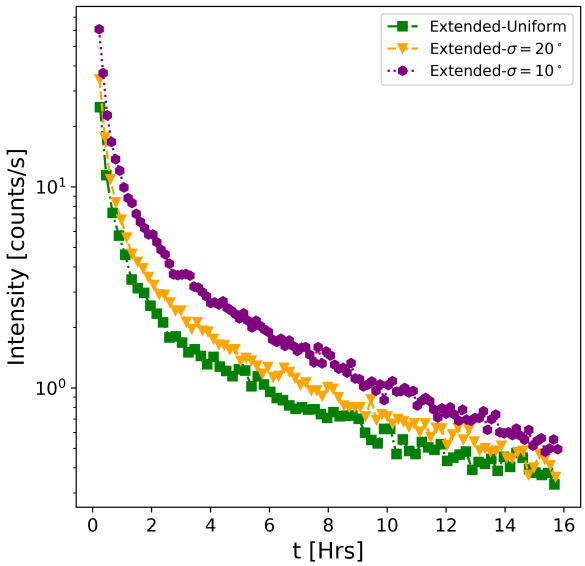

Figure 4: The intensity profiles at 1 au for the first 16 hours of simulations for time extended injections for a 25 x 25 degree collecting tile located at the initially magnetically well connected position (0°,0°). Green squares represent a uniform distribution, yellow triangles a Gaussian injection with $\sigma = 20°$ and purple hexagons a Gaussian injection with $\sigma = 10°$.

When we compare the intensity profiles away from the initially magnetically well-connected region (0°,0°) we find that there is significant longitudinal dependence, with the the most shock-nose

skewed injections having higher intensities for observers with footpoints westwards of (0°,0°) (right panels of Figure 5). The intensities at an observer connected eastwards of the initially magnetically well connected region have lower peak intensities and decay faster than the intensity profiles from the westward collecting tiles. This is likely the result of rapidly decreasing magnetic connectivity to the shock nose as the shock propagates radially and the flux tubes corotate with the Sun away from this observer. At eastern locations the injection with $\sigma = 10°$ has the lowest intensities. The intensities remain large southwards of the initially well connected region due to guiding centre drifts associated with gradient and curvature of the Parker spiral [3].

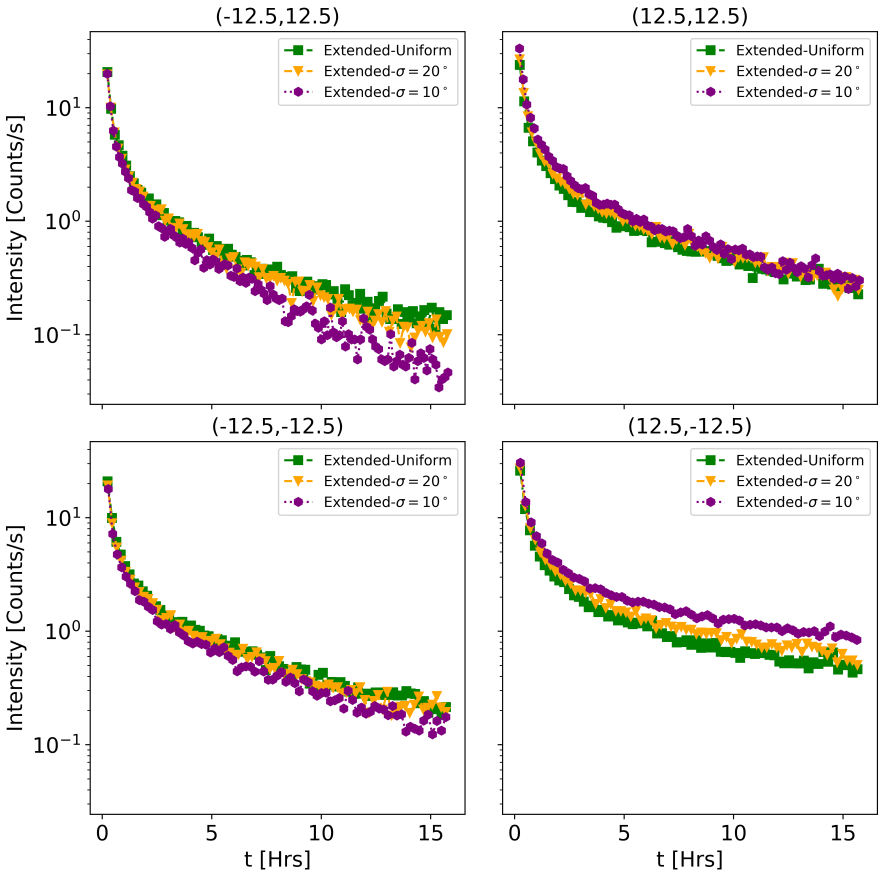

Figure 5: The intensity profiles at 1 au for the first 16 hours of simulations for time extended injections for 25 x 25 degree collecting tiles located at different positions relative to the initially magnetically well connected position (0°,0°), given by the titles of each panel. Green squares represent a uniform distribution, yellow triangles a Gaussian injection with $\sigma = 20°$ and purple hexagons a Gaussian injection with $\sigma = 10°$.

3.3 Intensity Profiles at 0.3 and 1 au

Figure 6 shows a comparison of intensity profiles at 0.3 and 1.0 au for the instantaneous-uniform injection (top left), extended-uniform (top right), extended-Gaussian ($\sigma = 10°$, bottom left) and extended-Gaussian ($\sigma = 20°$, bottom right). We consider a collecting tile of 50×50 degrees located at the initially magnetically well-connected region.

There is a significant difference between the instantaneous injection and the extended injections, with a larger peak intensity at 0.3 au and no rise phase for this time resolution in the instantaneous case. The first particles to arrive at the observer arrive scatter free. The extended injections with a peak at $t \sim 29.5$ minutes results in a rise phase of longer duration in the intensity profiles. In the instantaneous case peak injection occurs at $t = 0$. There are very different decay time constants for the 0.3 au and 1.0 au intensity profiles, with the 0.3 au intensity profiles decaying much faster than the intensity profiles at 1.0 au. The position and value of the peak intensities for all three extended injections are identical at 0.3 au for the position and size of the collecting tile used. We expect similar variations in longitude and latitude to that of Figure 5.

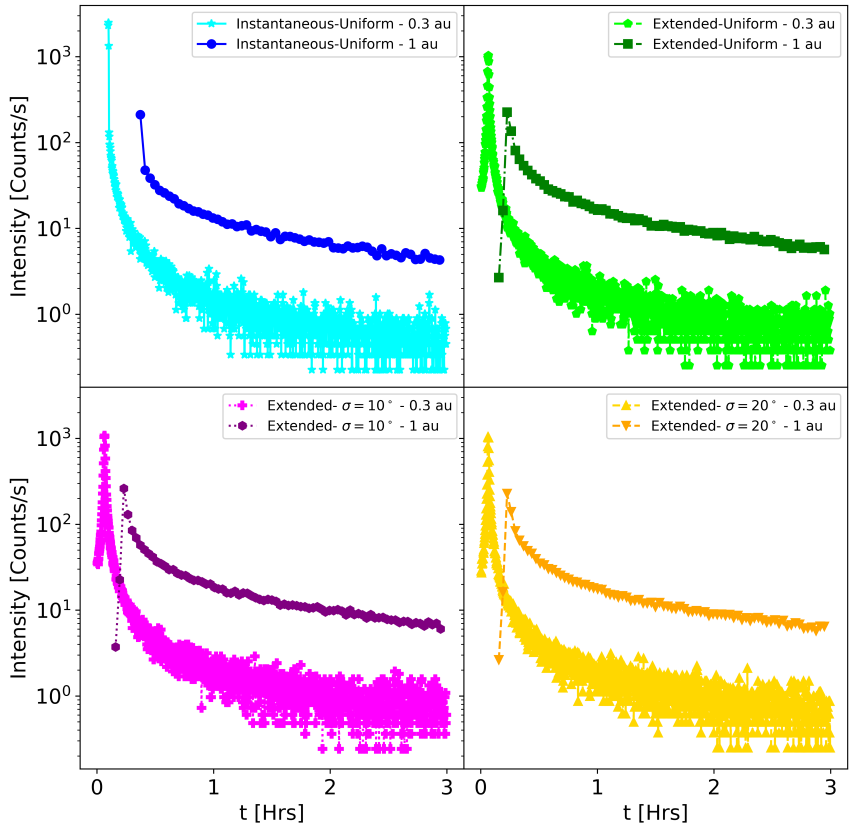

Figure 6: Intensity profiles for the first 3 hours of simulations with the four different injection scenarios at 0.3 au and 1.0 au, each considering a 50 x 50 degree collecting tile located at the initially magnetically well connected region (0°,0°).

4. Conclusions

We studied the effects of radially extended injections and the influence of different injection efficiencies across the shock front on the 0.3 and 1 AU intensity and anisotropy profiles for 100 MeV protons.

We find that compared to the case of an instantaneous injection, an extended particle injection causes slower decay phases in intensity profiles and slightly lower peak anisotropies, caused by

fewer focussed particles. However, the differences in the anisotropy profiles are only minor.

When considering injection efficiencies of different standard deviations across the shock, we found that a more shock-nose skewed injection results in larger intensities and slower decays measured at the initially magnetically well-connected region at 1 au. However, faster decays are observed eastwards of the initially magnetically well-connected position as fewer protons are injected into the flux tube due to the radial motion of the particle-injecting shock, which also reduces favourable magnetic connectivity with time and the flux tubes corotate away from the observer eastwards of the initially well-connected position.

The intensity profiles obtained at 0.3 au behave similarly for all extended injections, implying little dependence on how the particle acceleration efficiency changes in longitude and latitude across the shock front for the size of collecting tile used here.

Overall, significant differences in injection profiles in terms of duration (instantaneous versus extended) and efficiency along the shock (uniform, $\sigma = 20°$, $\sigma = 10°$) produce only small differences in observables at 1 au, for the energy (100 MeV) and the level of scattering considered ($\lambda = 1.0$ au).Therefore, the features that characterise the injections are difficult to determine observationally. Further work will be conducted to investigate protons of different energies, with different injection profiles.

References

[1] Battarbee, M., Dalla, S., and Marsh, M.S., (2018), ApJ, 854:23 (14pp), doi: 10.3847/1538-4357/aaafa

[2] Dalla, S., de Nolfo, G. A., Bruno, A., Giacalone, J., Laitinen, T., Thomas, S., Battarbee, M., and Marsh, M.S., (2020), A&A, 639, A105, doi: 10.1051/0004-6361/201937338

[3] Dalla, S., Marsh, M. S. , Kelly, J., Laitinen , T. (2013), JGR Space Physics , 118 , 5979 5985, doi:10.1002/jgra.50589

[4] Gopalswamy, N., Lara, A., Yashiro, S., Kaiser, M. L., and Howard, R. A., (2001), JGR: Space Physics, 106, 29207,doi: 10.1029/2001JA00017710.1029/2001JA000177

[5] Gopalswamy, N., Xie, H., Mäkelä, P., et. al. (2013), Adv.SpaceRes., 51,1981, doi:10.1016/j.asr.2013.01.00610.1016/j.asr.2013.01.006

[6] Marsh, M. S., Dalla, S., Kelly, J., and Laitinen, T., (2013), ApJ, 774:4, (9pp), doi:10.1088/0004-637X/774/1/4

[7] Reames, D., (2015) Space Sci Rev, 194:303–327, doi:10.1007/s11214-015-0210-7

[8] Wang, Y., Chen, C., Gui, B., Shen, c., Ye, P., and Wang, S., (2011), JGR, VOL. 116, A04104, doi:10.1029/2010JA016101

[9] Wang, Y., Qin, G., Zhang, M., (2012), ApJ, 752 37, doi:10.1088/0004-637X/752/1/37

[10] Zank, G. P., Li, G., Florinski, V., Hu, Q., Lario, D. and Smith, C. W., (2006), JGR, VOL. 111, A06108, doi:10.1029/2005JA011524